Chapter 11

Radiotherapy Dose Optimization in Target Tissues Using Internal Radiation-Generating Devices and Microspheres

Joseph John Bevelacqua

Additional information is available at the end of the chapter

http://dx.doi.org/10.5772/67203

Abstract

Preferentially delivering ionizing radiation to target tissues during radiotherapy procedures is investigated using internal radiation-generating devices and microspheres loaded with radioactive material. This chapter presumes the existence of internal radiation-generating devices and develops their requisite characteristics to permit the selective irradiation of tumors. The feasibility of disrupting a tumor's vascular structure is also investigated. Calculated absorbed dose profiles for both approaches demonstrate that dose can be successfully localized in a target tissue while minimizing the delivery to healthy tissue.

Keywords: absorbed dose, internal radiation-generating devices, microspheres, radiation therapy, tumor vascular disruption

1. Introduction

A significant issue associated with existing radiotherapy approaches is that agents that deliver dose to tumor cells also irradiate healthy tissue [1–6]. Short-term as well as long-term detriments can appear following radiotherapy procedures. These effects occur when healthy tissue outside the target volume is irradiated and affect the patient's subsequent recovery and quality of life. For example, short-term detriments (e.g., incontinence and erectile dysfunction) occur following prostate cancer therapy [7]. Long-term effects include secondary cancers and cardiovascular disease [8]. In view of these detriments, alternative therapy approaches that preferentially deliver dose to the target tissue are of interest and should be investigated.

This chapter considers two approaches that have the potential to significantly minimize the dose to healthy tissue while maximizing the dose delivered to the target tissue. The first technique utilizes internal radiation-generating devices that are in their conceptual development phase, and the second is an enhancement of the ^{90}Y microsphere approach that has been successfully utilized to treat liver cancers by disrupting the tumor's vasculature.

Heavy ions, neutrons, protons, and other radiation types have numerous applications for treating a variety of cancers [1–3, 6, 9–14]. To date, these techniques have focused on beams originating outside the body. These external beams selectively irradiate the tumor mass, but still deliver some dose to healthy tissue. This chapter investigates the possibility of using radiation-generating devices that would be implanted within a tumor to preferentially irradiate its volume and develops their requisite characteristics to permit the selective irradiation of tumors. These devices are postulated to have a size on the order of 10^{-6} m [1–3, 6].

Microspheres offer a unique approach that has the potential to impact tumor cells by disrupting their vascular structure. A number of authors [15, 16] have proposed a therapy approach that prevents the development of the tumor's vascular supply. Vascular disruption agents incorporate both chemotherapy [17, 18] as well as radiotherapy [18–27]. Radiotherapy vascular disruption techniques utilizing ^{90}Y microspheres, including anti-angiogenic and radioembolization therapies, are used to treat liver cancers [18–23]. Other radionuclides (e.g., ^{32}P) are under investigation, but radiation types other than high-energy beta particles are not under active consideration [22].

2. Internal radiation-generating devices

The requisite technology to construct internal radiation-generating devices (IRGDs) is being developed (e.g., electron accelerators powered by lasers [28]). These devices are optical cavities [28] whose size depends on the laser's wavelength. The utilization of shorter wavelength lasers leads to devices of the size envisioned for IRGDs [1–3, 6].

Refs. [1–6] provide calculations for the range of heavy ions in water. By selecting appropriate ion and energy combinations, specific target irradiation locations are preferentially irradiated. The capability to localize dose in the target is a positive feature that makes heavy ions an attractive tool for external beam therapy and supports their potential use in an IRGD. By adjusting the beam energy and radiation type, an IRGD has the capability to selectively irradiate the tumor.

2.1. Candidate radiation types

Internal devices could incorporate pions, muons, photons, electrons, protons, and heavy ions to deposit energy into tumors. Ranges on the order of a centimeter are achieved using 10–20 MeV pions and muons, 30–40 MeV protons, 100–200 MeV alpha particles, and energies on the order of 90 MeV/nucleon for ^{12}C, ^{16}O, ^{20}Ne ions, and heavier ions [1–6].

http://dx.doi.org/10.5772/67203

2.2. IRGD characteristics and arrangement

The feasibility of using IRGDs for therapy applications is illustrated using a cubic Cartesian configuration. This configuration is repeated to irradiate various tumor sizes. A unit cell concept is arbitrary, but simplifies the calculation of absorbed dose to the tumor site.

The cubic Cartesian configuration utilizes 27 devices arranged in three planes with nine devices in each plane. The coordinates of the devices are written in terms of a scaled dimension ξ:

$$\xi = \frac{R}{d} \tag{1}$$

where d is the internal device grid spacing and R is the maximum ion range. This approach facilitates a general discussion and eliminates adjustments for specific ion-energy combinations.

The 27 devices reside at the locations (x, y, z): (0, 0, z), (ξ, 0, z), (ξ, − ξ, z), (0 − ξ, z), (−ξ, − ξ, z), (−ξ, 0, z), (−ξ, ξ, z), (0, ξ, z), and (ξ, ξ, z) for z = -ξ, 0, and ξ. Utilizing additional devices enhances the delivery of dose in a more uniform manner.

IRGDs should incorporate a number of characteristics to facilitate the dose delivery to the target volume. In general, the IRGDs should have the capability to (1) irradiate 4π steradians, (2) deliver various ion-energy combinations, (3) be controlled in real time, (4) rapidly change the radiation type, energy, and fluence, (5) produce a variable fluence to deliver a uniform dose, (6) position itself at a desired location, (7) monitor the delivered dose profile using positron emission tomography or other techniques to verify that it is preferentially irradiating the tumor volume, and (8) have the capability to be removed from the body.

Delivering a uniform absorbed dose (D) requires careful control of the fluence, ion type, and energy (E). These parameters are varied during the irradiation time (T) to deliver a uniform dose within the unit cell:

$$D=\sum_{i=1}^{N}\int_{-\xi}^{+\xi}\int_{-\xi}^{+\xi}\int_{0}^{+\xi}\int_{0}^{T}\frac{1}{\rho(x_i,y_i,z_i)}\left(-\frac{dE(x_i,y_i,z_i,t)}{dr(x_i,y_i,z_i)}\right)\times\dot{\Phi}\left(x_i,y_i,z_i,t\right)dx_i\,dy_i\,dz_i\,dt \tag{2}$$

where $r(x_i, y_i, z_i)$ is the distance measured from each device, $\Phi(x_i, y_i, z_i, t)$ is the time-dependent fluence rate, *N* is the number of implanted devices, and *i* labels the individual device [1–3, 6].

2.3. Absorbed dose calculations

Eq. (2) is used to calculate the absorbed dose from internal radiation-generating devices within a Cartesian lattice. Stopping powers are determined using the methodology outlined in Refs. [1–6], and energy-dependent cross sections are obtained from Shen et al's parameterization [29] or models [1–6].

As an initial example of the internal device concept, a spectrum of eight proton groups (i.e., 10, 20, 30, 40, 50, 60, 70, and 80 MeV) is selected to be the output of the device. A spectrum of energies facilitates the irradiation of the entire tumor volume. A uniform distribution of

proton dose requires a continuous proton energy distribution. The 27 proton generating devices are distributed in a 10 × 10 × 10 cm volume of water. Each device is assumed to radiate isotropically. The results of irradiating this water volume with 27 internal devices generating an output of 10, 20, 30, 40, 50, 60, 70, and 80 MeV protons are illustrated in **Figure 1**. The fluence at each proton energy is selected to be the same.

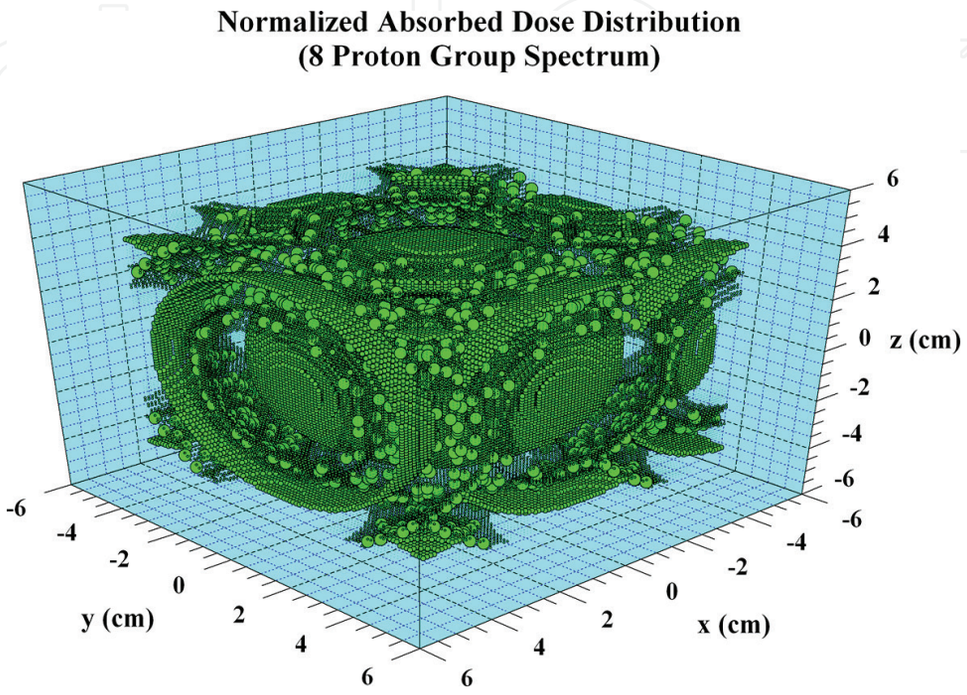

Figure 1. Normalized absorbed dose distribution from 27 internal radiation-generating devices producing a spectrum of eight proton groups (i.e., 10, 20, 30, 40, 50, 60, 70, and 80 MeV protons). The absorbed dose is proportional to the plotted circle radius.

Since the total absorbed dose of **Figure 1** is the superposition of a number of manifolds (i.e., the various isodose surfaces), the structure of the surface is governed by the proton output spectrum, fluence, attenuating medium characteristics, ion stopping power, and reaction cross section as noted in Eqs. (1) and (2). **Figure 1** represents the three-dimensional absorbed dose profile. In **Figure 1**, the dose at each point is proportional to the plotted circle radius.

Figure 1 illustrates the symmetry of the absorbed dose distribution associated with the 27 internal radiators. Although the distribution is not uniform, the IRGDs effectively irradiate the target volume. The average dose to the target 10 × 10 × 10 cm volume depends on the IRGD proton spectrum. For example, proton energy groups of 10 MeV; 10 and 20 MeV; 10, 20, 30, and 40 MeV; and 10, 20, 30, 40, 50, 60, 70, and 80 MeV produce to an average dose over the target volume of 5.89×10^{-6}, 5.75×10^{-4}, 3.00×10^{-2}, and 9.79×10^{-2} relative to the peak dose, respectively.

Increasing the number of proton energy groups between 10 and 80 MeV range will continue to increase the average absorbed dose to the tumor site. The discussion of the characteristics of the detailed three-dimensional absorbed dose profile illustrates the complexity of therapy planning when implementing a new technology.

http://dx.doi.org/10.5772/67203

3. Radionuclide vascular disruption therapy using microspheres

Conventional radiotherapy often involves the deposition of the radionuclide within a tumor mass. It is also feasible to attack the tumor by disrupting its blood supply. Vascular disruption agents have been developed and utilized in chemotherapy and radiotherapy.

3.1. Tumor vasculature

The vascular structure of normal tissue provides an efficient method to deliver nutrients. Growing tumors have a poorly developed vasculature that does not adequately nourish the cells [17]. The tumor's weak vascular structure can be degraded using a chemical or radioactive agent.

Vessels that are dilated and have elongated shapes, blind ends, bulges, leaky sprouts, and abrupt diameter changes are defects that occur in a tumor's vascular structure. These vessel defects create sluggish and irregular blood flow that poorly nourish cancer cells and result in hypoxic tumors. Hypoxic conditions limit the effectiveness of both chemotherapy and radiotherapy and provide a measure of radioresistance to tumor cells when compared to normal, oxygenated cells. Since a tumor's growth is dependent on sufficient nourishment, eliminating its blood supply provides an additional opportunity to facilitate its destruction [17].

3.2. Current radiological efforts

Radiological efforts at tumor vascular disruption have focused on ^{90}Y. ^{90}Y was a logical choice for anti-angiogenic therapy since the dose to destroy a tumor is ≥70 Gy. However, the 2.27 MeV ^{90}Y beta particles have a range in tissue of about 1.1 cm, which deposits dose to healthy tissue well beyond the target vasculature. Bremsstrahlung from the ^{90}Y beta particles provides additional dose to healthy tissue. The properties of ^{90}Y microspheres used in therapy applications are summarized by Kennedy et al. [22].

Medical reviews suggest that the ^{90}Y approach is a safe and effective therapy method for selected patients. However, a number of negative features are associated with ^{90}Y microsphere therapy [22]. First, ^{90}Y bremsstrahlung affects healthy tissue well beyond the vasculature. Second, resin microspheres may have trace ^{90}Y on their surface, which is excreted through urine. As the ^{90}Y is excreted, additional absorbed dose is delivered to healthy tissues. Third, the total dose delivered to the lung should not exceed 30 Gy to prevent radiation pneumonitis. Fourth, patients can exhibit abdominal pain, fatigue, and nausea within three days posttreatment. Fifth, dose delivered to healthy tissue causes acute damage that includes pancreatitis, gastrointestinal ulceration, and radiation pneumonitis. Radiation-induced liver disease is a possible late effect of ^{90}Y microsphere therapy.

3.3. Theoretical methodology

A tumor's blood supply is reduced by a vascular disruption agent that causes the vessel wall to become restricted or breached to increase leakage. IRGDs and microspheres using alpha-

emitting radionuclides (MAs) preferentially deliver absorbed dose to the blood vessel wall to facilitate its disruption. The wall thicknesses for a variety of human blood vessel types [30] are summarized in **Table 1**.

Blood vessel type	Wall thickness	Lumen diameter
Aorta	2 mm	25 mm
Artery	1 mm	4 mm
Arteriole	20 μm	30 μm
Capillary	1 μm	8 μm
Venule	2 μm	20 μm
Vein	0.5 mm	5 mm
Vena Cava	1.5 mm	30 mm

[a]Barrett et al. [30].

Table 1. Characteristics of various blood vessel types[a].

Tumor vessel wall sizes, including arterioles, are usually <100 μm [17]. Although arterioles are used as the base case in this chapter, the vessel sizes summarized in **Table 1** suggest that a variety of blood vessel types could service a developing tumor [30].

3.4. Microsphere radionuclide selection and characteristics

An alternative to the use of ^{90}Y is provided by radionuclides that emit low-energy photons, low-energy beta particles, or alpha particles. These radionuclides would replace ^{90}Y as the radioactive material loading the microspheres.

Desirable characteristics for the radionuclide and candidate microsphere to facilitate tumor blood vessel disruption include the (1) nuclide has a short effective half-life, (2) range of the emitted radiation is <100 μm or the maximum vessel wall thickness, (3) arteriole wall dose is at least 100 Gy, (4) healthy tissue dose is minimized, (5) microsphere preferentially attaches to the wall of the tumor's arteriole, (6) candidate radionuclide is compatible with the microsphere, and (7) the microsphere can be removed from the body at a desired time.

Although these characteristics provide a basis for the calculations presented in this chapter, they have not been optimized to produce a viable alternative to the ^{90}Y microsphere approach. As noted in Refs. [4–6], both alpha-emitting and low-energy beta-gamma loaded microspheres can be utilized to disrupt a tumor's vasculature. However, the daughter radiation presents a problem, and this radiation can often irradiate healthy tissue that was an original concern associated with the ^{90}Y approach.

Production challenges and associated availability are impediments for the use of alpha-emitting radionuclides. Therefore, the availability of the selected radionuclide is an important

http://dx.doi.org/10.5772/67203

consideration. ^{222}Rn is readily available and would be a candidate for microsphere use. The ^{222}Rn daughters yield additional dose to the tumor vasculature, which could enhance the approach if healthy dose is avoided.

3.4.1. Selection of radionuclide

In Refs. [4–6], a list of candidate alpha- and beta-gamma-emitting radionuclides was created. Unfortunately, most candidate radionuclides, including ^{149}Tb, ^{211}At, ^{212}Bi, ^{213}Bi, ^{223}Ra, ^{225}Ac, and ^{227}Th, have daughter gamma, beta, or bremsstrahlung radiation that irradiates healthy tissue well beyond the target volume, which does not meet the goal of minimizing the dose delivered beyond the arteriole wall. As part of that goal, ^{222}Rn was noted as an interesting possibility since it occurs naturally as part of the ^{238}U decay chain. Eq. (3) lists the ^{222}Rn decay daughters with the associated decay scheme:

$$^{222}\mathrm{Rn} \xrightarrow{\alpha} {}^{218}\mathrm{Po} \xrightarrow{\alpha} {}^{214}\mathrm{Pb} \xrightarrow{\beta^-} {}^{214}\mathrm{Bi} \xrightarrow{\beta^-} {}^{214}\mathrm{Po} \xrightarrow{\alpha} {}^{210}\mathrm{Pb} \xrightarrow{\beta^-} {}^{210}\mathrm{Bi} \xrightarrow{\beta^-} {}^{210}\mathrm{Po} \xrightarrow{\alpha} {}^{206}\mathrm{Pb} \tag{3}$$

Although ^{222}Rn has a number of desirable characteristics, its daughters emit beta and gamma radiation that deliver absorbed dose well beyond the thickness of the arteriole wall. Therefore, ^{222}Rn is not a primary candidate to achieve selective dose delivery to the vascular wall. However, a review of the ^{222}Rn daughters suggests that ^{210}Po has the desired characteristics for vascular disruption without significantly irradiating healthy tissue. In particular, the ^{210}Po 5.3 MeV alpha particle irradiates the arteriole wall and limits the absorbed dose beyond the target tissue. In addition, the weak 803 keV ^{210}Po photon radiation with a yield $<1.0 \times 10^{-3}$% delivers minimal dose beyond the target tissue.

3.4.2. Basic microsphere design

The base case microsphere is loaded with 0.3 Bq of ^{210}Po uniformly distributed in a 1-μm-diameter ^{12}C sphere having a density of 2.0 g/cm^3. Subsequent discussion provides the basis for the 0.3 Bq activity.

Subsequent discussion is based on a single microsphere. However, treatment procedures will utilize many spheres with the actual number determined by the cancer type and its progression. Although microsphere delivery methods other than the usual catheter approach [2–6] may be feasible, initial efforts will likely focus on the traditional delivery method [17–23].

3.4.3. Absorbed dose computational model

A ^{210}Po activity of 0.3 Bq delivers an absorbed dose of about 100 Gy to the arteriole wall. Defining a more exact activity value is not necessary because the design has yet to be refined. The activity value also depends on the insertion and removal methods, fabrication details, and relative biological effectiveness values for the ^{210}Po alpha and gamma radiation.

3.4.3.1. Absorbed dose from alpha particles

The absorbed dose (*D*) delivered by ions of a specific energy as a function of penetration distance *x* into tissue is [1, 12]:

$$D(x) = \frac{1}{\rho}\left(-\frac{dE}{dx}\right)\Phi(x) \tag{4}$$

where ρ is the density of tissue attenuating the ion, −dE/dx is the stopping power, and Φ(x) is the alpha particle fluence at the location of interest. The particle fluence varies with tissue penetration depth according to the relationship:

$$\Phi(x) = \Phi(0)\, e^{-\Sigma x} \tag{5}$$

where Φ(0) is the entrance fluence and Σ is the macroscopic reaction cross section. Alpha particle stopping powers are derived from Bethe's formulation [31] and follow an approach similar to the SPAR code [32]. The energy-dependent cross sections are obtained from Shen et al's parameterization [29] or models [1–6].

3.4.3.2. Photon absorbed dose

The photon absorbed dose is derived from the standard point source relationships [4–6]:

$$D = \frac{S}{4\pi r^2}\frac{\mu_{en}}{\rho} E\, B(\mu x)\, e^{-\mu x} \tag{6}$$

where S is the total number of photons irradiating the arteriole wall, r is the distance from the microsphere, μ_{en}/ρ is the mass-energy absorption coefficient, E is the photon energy, B is a buildup factor, and μ is the attenuation coefficient. The gamma absorbed dose contribution is obtained from the ISO-PC computer code [33]. Requisite photon data for ^{210}Po are based on Rittman [33].

3.4.4. Relative biological effectiveness

In therapy applications, the absorbed dose is multiplied by the relative biological effectiveness (RBE) to reflect the cell killing efficiency of a radiation type. The RBE of radiation type x is defined as the ratio of the dose of a reference energy photon to produce an effect and the dose of radiation type x to produce the same biological effect. Although the RBE is a simple concept, its therapy application is complex [34], because the RBE depends on a number of factors. These include the radiation type and its energy, the delivered absorbed dose, the delivery method (e.g., dose fractionization sequence), and the irradiated cell and tissue types. No RBE is applied to the absorbed doses calculated in this chapter because the design of the ^{210}Po microsphere is being developed. However, the alpha particle RBE is greater than unity. Therefore, the calculated absorbed doses for tumor disruption represent a lower bound for the dose delivered by the ^{210}Po microsphere.

http://dx.doi.org/10.5772/67203

3.4.5. Microsphere results and discussion

In subsequent discussion, the ^{210}Po microsphere resides at the inner wall of an arteriole. **Figures 2** and **3** illustrate absorbed dose profiles for water thicknesses ≤100 μm. Following previous work, the vessel wall is assumed to be water that is a good approximation for tissue [1–6, 12].

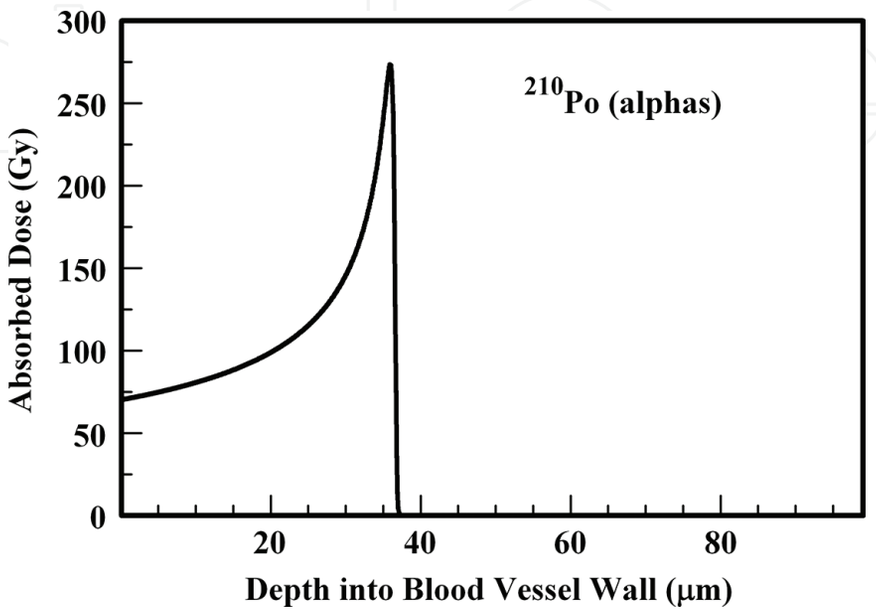

Figure 2. Absorbed dose profile for ^{210}Po alpha particles in a water medium. The absorbed dose is delivered by 0.3 Bq of ^{210}Po uniformly deposited within a 1-μm-diameter microsphere following the total decay of the radioactive material.

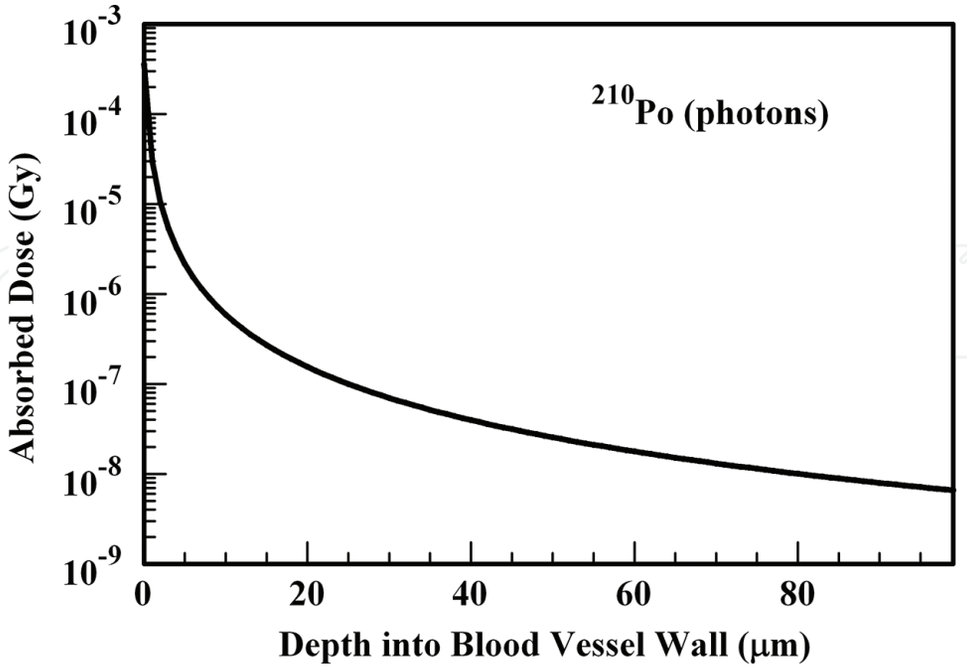

Figure 3. Absorbed dose profile for ^{210}Po photons in a water medium. The absorbed dose is delivered by 0.3 Bq of ^{210}Po uniformly deposited within a 1-μm-diameter microsphere following the total decay of the radioactive material.

Figures 2 and **3** provide the results of alpha and gamma contributions to the absorbed dose from a ^{210}Po microsphere, respectively. Since the gamma absorbed dose is significantly less than the alpha absorbed dose, **Figure 2** represents the total absorbed dose delivered by the ^{210}Po MA.

Since the peak dose is delivered at 35.9 μm, the 100 μm dose localization value is achieved. At the Bragg peak, the alpha to gamma dose ratio is 1.7×10^{10}. Beyond the Bragg peak, ^{210}Po photons deliver less than 0.1 μGy. Although ^{210}Po MAs achieve the desired dose localization, its longer half life (138 d) relative to ^{32}P (14.28 days) and ^{90}Y (2.669 days) [35] must be addressed.

The time (t)-dependent dose rate to the arteriole wall is given by the relationship:

$$\dot{D}(t) = \dot{D}(0)\, e^{-\lambda t} \tag{7}$$

where λ is the physical decay constant of the radionuclide. Integrating Eq. 7 yields the total dose at time T:

$$D(T) = \frac{\dot{D}(0)}{\lambda}(1 - e^{-\lambda T}) = D(\infty)\,(1 - e^{-\lambda T}) \tag{8}$$

Since the activity is proportional to the delivered dose, early removal of the microsphere at time T requires an increase in the initial activity loading by a factor (F), which is the ratio of D(∞)/D(T) [5]:

$$F = \frac{1}{(1 - e^{-\lambda T})} \tag{9}$$

This activity increase delivers the required dose to disrupt the microsphere as noted in **Figures 2** and **3**. For example, an activity of about 2 Bq (0.3 Bq × 7.19) is the requisite ^{210}Po activity loading to produce the doses summarized in **Figures 2** and **3** if the microspheres are removed at 30 days (F(30 days) = 7.19).

3.4.6. Microsphere delivery methods

In initial studies, a catheter will introduce the MA into the tumor vasculature. Following the methodology developed in ^{90}Y microsphere liver cancer therapy, the catheter enters through the femoral artery into the liver and deposits the microspheres into the tumor's blood vessels. Image-guided radiation therapy [26, 36] facilitates guiding the catheter to specifically target the tumor vasculature.

The catheter delivery method could be utilized in the treatment of a number of tumors. Specific catheter paths for the various tumor types will be refined and developed in a manner that was similar to the evolution of the ^{90}Y microsphere treatment of liver cancers [17–23]. For example, renal artery access would facilitate ^{210}Po MA deposition into the vasculature of kidney tumors.

Developing a method for preferentially depositing the MA into the desired blood vessel requires additional research and development. The microsphere research and design effort

http://dx.doi.org/10.5772/67203

should investigate a number of chemical and physical approaches. These approaches include the use of electric charge, heat, pH, and electromagnetic fields to achieve the desired attachment of the MA to the tumor's vascular wall. The specific design options that require experimental effort include the MAs (1) electric charge and its spatial distribution, (2) dielectric and diamagnetic characteristics, (3) physical size and shape, and (4) material composition. Activating agents could be used to optimize the MA design. Electromagnetic fields heat, lasers, and a spectrum of electromagnetic radiation are possible activating agents.

3.4.7. Microsphere removal methods

Eqs. (7)–(9) suggest that extraction of MAs at a specified time requires the development of removal mechanisms. Removal could be accomplished by reversing the delivery methods discussed previously. For example, deposition and removal could be achieved by incorporating a magnetic material in the MA. The magnetic particles facilitate placement in the desired location using an active, localized magnetic field. Eliminating the magnetic field would facilitate microsphere removal. The protocol for microsphere implantation and removal requires additional research and development.

3.4.8. Effective half-life

As noted previously, the ^{210}Po physical half-life (T_p) must be addressed before the MA therapy application becomes a reality. The physical half-lives of ^{210}Po and ^{90}Y are 138 and 2.7 days, respectively. A ^{90}Y delivery approach will not be successful for ^{210}Po if the MA design does not shorten the biological half-life of the device.

In the case of the shorter half-life ^{90}Y, some microspheres are transported via blood into the lung and irradiate healthy tissue. Since the physical half-life of ^{90}Y is short, this deposition yields a relatively insignificant dose. Assuming the same transfer characteristics, ^{210}Po produces a larger lung dose and could create a significant biological detriment. This concern is eliminated if the ^{210}Po MA design produces a shorter biological half-life in the lung.

In view of these considerations, constructing ^{210}Po MAs with a short effective half-life is a design requirement. For example, the ^{210}Po MAs could be constructed using a material having ICRP 30 [37] Class D lung retention characteristics. Following the ICRP 30 methodology, Class D materials have a biological half-life <10 days. Part of ^{210}Po MA development is the use of a material with a short biological half-life. The ^{210}Po MA effective half-life in the lung is [38]:

$$T_e = \frac{T_p\, T_b}{T_p + T_b} \tag{10}$$

Following Eq. (10), the effective half-life (T_e) of a radionuclide depends on its biological and physical half-lives. Therefore, a long physical half-life is not a limiting factor if the biological half-life (T_b) is short. For example, the ^{210}Po effective half-life for a material with 2- and 10-day biological half-lives is 1.97 and 9.32 days, respectively. A MA design requirement for a Class D biological half-life eliminates the longer ^{210}Po physical half-life concern.

3.4.9. ^{210}Po toxicity and patient safety

^{210}Po has a specific activity of 1.7×10^{14} Bq/g, and its inhalation (ingestion) effective dose coefficient (EDC) is 3.0×10^{-6} Sv/Bq (2.4×10^{-7} Sv/Bq) [39]. The intake pathway caused by MA leaching has not been evaluated. In view of the inhalation and ingestion EDCs, the leaching EDC is probably in the range of the established conventional intake pathway values. For an initial scooping assessment, the leaching EDC is approximately 10^{-6} Sv/Bq. Considering the proposed 0.3 Bq ^{210}Po MA, complete ^{210}Po leaching from a single microsphere produces to an effective dose of about 0.3 μSv.

The effective dose from complete MA leakage is mitigated if the microspheres have good retention characteristics. With good ^{210}Po retention characteristics, the radiological hazard to the patient is not significant. For example, if 10^6 0.3 Bq MAs were administered with a ^{210}Po retention of 90%, the patient's 50-year effective dose commitment is only 30 mSv.

4. Vascular disruption using internal radiation-generating devices

Vascular disruption can also be achieved using internal radiation-generating devices. These devices meet the desired characteristics to maximize dose to the tumor's vascular walls while minimizing the dose to healthy tissue. For a tissue volume irradiated by a beam of ions of a given energy, the absorbed dose (D) as a function of penetration distance into tissue is given by Eqs. (4) and (5). Arteriole vascular disruption is outlined for beams of protons, alpha particles, and ^{12}C, ^{20}Ne, and ^{40}Ca ions. All beams were assumed to be fully ionized (e.g., ^{12}C ions have a +6 e charge).

The photon absorbed dose is derived from Eq. (6). Because higher energy photons have poor dose localization, low-energy photons are investigated as a possible vascular disruption agent.

4.1. Internal radiation-generating device results and discussion

The base case considered in this chapter is the 20 μm arteriole wall thickness. With this emphasis, the dose delivered to the arteriole wall and blood vessel wall thicknesses ≤100 μm [17] is calculated. The target dose, which is about of 100 Gy, is sufficient to disrupt the vessel wall. Dose delivery has not been optimized, and ion fluences to reach the 100 Gy dose level are 5×10^9, 5×10^8, 1×10^8, 5×10^7, and 1×10^7 ions/cm^2 for protons, alpha particles, ^{12}C, ^{20}Ne, and ^{40}Ca, respectively. 1×10^{10} photons are utilized in the calculations using Eq. (6).

In subsequent absorbed dose calculations, the internal radiation-generating device is assumed to reside at the inner arteriole wall. **Table 2** summarizes the calculations for photons, protons, alpha particles, and ^{12}C, ^{20}Ne, and ^{40}Ca ions and compares these results with beta-emitting nuclides currently used in therapy applications. To further illustrate the internal radiation-generating device concept, **Figure 4** illustrates the ^{12}C absorbed dose profiles for blood vessel wall depths ≤100 μm. The ^{12}C energies included in **Figure 4** are 10, 20, 25, 30, 40, and 50 MeV. Water is assumed to be the medium comprising the vessel wall.

http://dx.doi.org/10.5772/67203

Radionuclide or radiation delivery approach	Radiation type emitted	Range (μm)	E (MeV)
^{90}Y	β^-	1.1×10^4	2.281[a]
^{32}P	β^-	7.9×10^3	1.709[a]
^{33}P	β^-	5.9×10^2	0.249[a]
^{35}S	β^-	3.2×10^2	0.1674[a]
IRGD[b]	p	10–95	0.5–2.3
IRGD[b]	α	15–75	3.0–8.0
IRGD[b]	^{12}C	5–90	10.0–50.0
IRGD[b]	^{20}Ne	10–85	30.0–110.0
IRGD[b]	^{40}Ca	10–75	100.0–300.0
IRGD[b]	γ	0–20[c]	0.015–0.050
IRGD[b]	γ	0–70[d]	0.015–0.050

[a]Maximum beta energy.

[b]Internal radiation-generating device (IRGD).

[c]The dose decreases by a factor of about 10^3 over the listed depths.

[d]The dose decreases by a factor of about 10^4 over the listed depths.

Table 2. Dose localization for candidate radionuclides and radiation types.

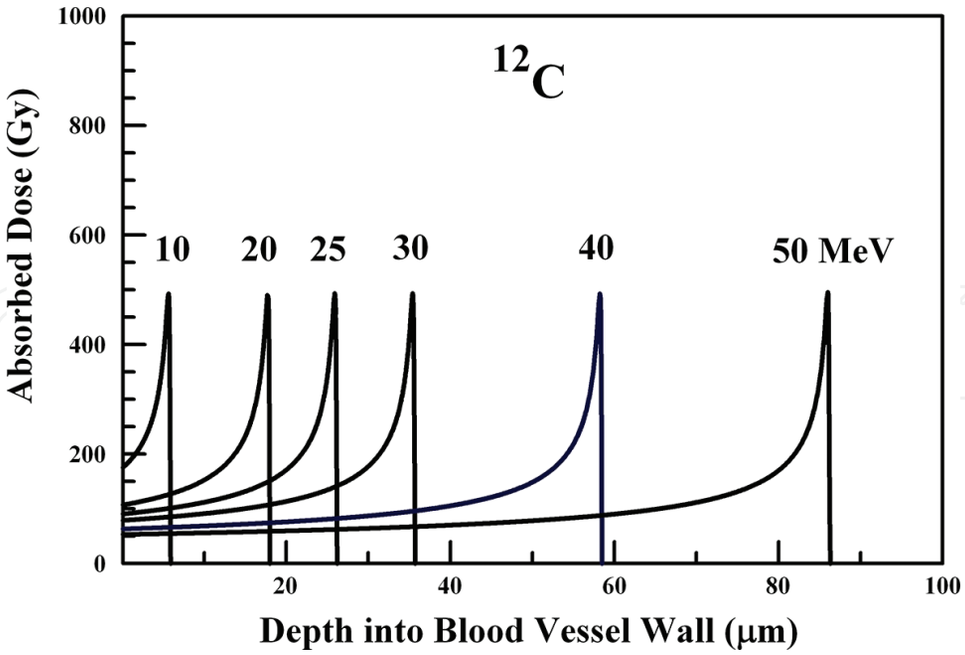

Figure 4. Absorbed dose profiles for ^{12}C ions in water. The absorbed dose curves peak at a greater depth with increasing ^{12}C ion energy. The total ion fluence for all energies is 1.0×10^8 ^{12}C ions/cm^2. The ions are delivered by an internal radiation-generating device.

Dose localization within an arteriole wall could be achieved using 1.0–1.5 MeV proton beams. Alpha particles with energies below 3 MeV will not penetrate the arteriole wall. The arteriole wall is disrupted, with minimal dose to surrounding tissue, by alpha particles in the 4–5 MeV energy range. Sufficient absorbed dose to disrupt vessels with wall thicknesses between 20 and 100 μm can be delivered by alpha particles having energies below 8 MeV.

^{12}C ions with energies below about 20 MeV do not penetrate the arteriole wall, and 20–50 MeV ions will deposit sufficient energy into a range of vessel wall thicknesses in the 20–100 μm range to produce vascular disruption. Selective arteriole wall disruption is achieved using 25–30 MeV ^{12}C ions. However, the generation of ^{12}C, ^{20}Ne, and ^{40}Ca ions is a more significant technical challenge than producing lighter ions in a first generation IRGD.

^{20}Ne ions below 30 MeV do not penetrate the arteriole wall. ^{20}Ne ions in the range of 50–110 MeV will be sufficient to reach the range of vessel wall thicknesses addressed in this chapter. Arteriole wall disruption with minimal dose to surrounding tissue is achieved using 50–70 MeV ^{20}Ne ions. In a similar manner, ^{40}Ca ions require 150–200 MeV to selectively disrupt the arteriole wall and 100–300 MeV ^{40}Ca ions penetrate vessel wall thicknesses of 10–75 μm.

Table 2 illustrates that photon energies in the range of 15–50 keV can deposit the requisite absorbed dose to disrupt an arteriole wall. Significant dose is also deposited in the 20–100 μm range by the 15–50 keV photons. However, protons and ^{4}He, ^{12}C, ^{20}Ne, and ^{40}Ca ions achieve better dose localization.

Internal radiation-generating devices can also be developed to emit low-energy electrons. Electrons present a concern because their bremsstrahlung radiation can irradiate healthy tissue beyond the target volume. However, low-energy electrons preferentially irradiate the arteriole wall with minimal bremsstrahlung. **Table 3** summarizes the range and bremsstrahlung production for 20–85 keV electrons impinging on the arteriole wall.

Electron energy (keV)	Range in water (μm)	Fraction of electron energy converted into bremsstrahlung
20	6.79	5.26×10^{-5}
25	10.6	6.57×10^{-5}
30	15.1	7.89×10^{-5}
35	20.3	9.20×10^{-5}
40	26.1	1.05×10^{-4}
50	39.6	1.31×10^{-4}
60	55.1	1.58×10^{-4}
70	72.6	1.84×10^{-4}
80	91.8	2.10×10^{-4}
85	102	2.23×10^{-4}

Table 3. Vascular disruption by low-energy electrons from an internal radiation-generating device.

The results summarized in **Table 3** suggest that 35–40 keV electrons also offer the potential to selectively disrupt an arteriole servicing a tumor. Dose localization is achieved with minimal bremsstrahlung production that permits vascular disruption without delivering absorbed dose to healthy tissue. **Table 3** also illustrates that electrons below 85 keV also selectively irradiate vessel wall thicknesses below 100 μm.

5. Conclusions

Internal radiation-generating devices and microspheres loaded with alpha-emitting radionuclides preferentially deposit dose in the target tissues while minimizing the dose delivered to healthy tissue. This selective deposition minimizes stray dose and limits the side effects that often accompany radiotherapy procedures. The microsphere approach can be realized in the near term, but an internal radiation-generating device relies on technology that is not currently available. Additional research is required to develop the techniques proposed in this chapter into practical radiotherapy protocols.

Author details

Joseph John Bevelacqua

Address all correspondence to: bevelresou@aol.com

Bevelacqua Resources, Richland, WA, USA

References

[1] Bevelacqua JJ. Systematics of heavy ion radiotherapy. Radiation Protection Management. 2005;**22(6)**:4–13.

[2] Bevelacqua JJ. Feasibility of using internal radiation-generating devices in radiotherapy. Health Physics. 2010;**98**:614–620. doi:10.1097/HP.0b013e3181c8f6ac

[3] Bevelacqua JJ. Angular absorbed dose dependence of internal radiation-generating devices in radiotherapy. Health Physics. 2012;**102**:2–7. doi:10.1097/HP.0b013e318227e80d

[4] Bevelacqua JJ. Tumor vascular disruption using various radiation types. PeerJ. 2014;**2**:e320. doi:10.7717/peerj.320

[5] Bevelacqua JJ. ^{210}Po microsphere radiological design for tumor vascular disruption. PeerJ. 2015;**3:**e1143. doi:10.7717/peerj.1143

[6] Bevelacqua JJ. Health physics: radiation-generating devices, characteristics, and hazards. Weinheim: Wiley-VCH; 2016. 800 p.

[7] Martinez AA, Gonzalez JA, Chung AK, Kestin LL, Balasubramaniam M, Diokno AC, Ziaja EL, Brabbins DS, Vicini FA. A comparison of external beam radiation therapy versus radical prostatectomy for patients with low risk prostate carcinoma diagnosed, staged and treated at a single institution. Cancer. 2000;**88**:425–432. doi:10.1002/(SICI)1097-0142(20000115)88:2<425::AID-CNCR25>3.0.CO;2-Z

[8] NCRP Report No. 170. Second primary cancers and cardiovascular disease after radiation therapy. 2012; Bethesda: NCRP Publications.

[9] Johns HE, Cunningham JR. The physics of radiology, 4th ed. Springfield, IL: Charles C. Thomas Publisher; 1983. 796 p.

[10] Hirao Y, Ogawa H, Yamada S, Sato Y, Yamada T, Sato K, Itano A, Kanazawa M, Noda K, Kawachi K, Endo M, Kanai T, Kohno T, Sudou M, Minohara S, Kitagawa A, Soga F, Takada E, Watanabe S, Endo K, Kumada M, Matsumoto S. Heavy ion synchrotron for medical use—HIMAC project at NIRS-Japan. Nuclear Physics. 1992;**A538**:541c–550c.

[11] Scheidenberger C, Geissel H. Penetration of relativistic heavy ions through matter. Nuclear Instruments and Methods in Physics Research Section B: Beam Interactions with Materials and Atoms. 1998;**135**:25–34.

[12] Kraft G. Tumor therapy with heavy charged particles. Progress in Particle and Nuclear Physics. 2000;**45**:S473–S544. doi:10.1016/S0146-6410(00)00112-5

[13] Akabani G, Kennel SJ, Zalutsky MR. Microdosimetric analysis of particle-emitting targeted radiotherapeutics using histological images. Journal of Nuclear Medicine. 2003;**44**:792–805.

[14] Li Q, Furusawa Y, Kanazawa M, Kanai T, Kitagawa A, Aoki M, Urakabe E, Sate S, Wei Z. Enhanced biological effect induced by a radioactive ^{9}C-ion beam at the depths around its Bragg peak. Nuclear Instruments and Methods in Physics Research Section B: Beam Interactions with Materials and Atoms. 2006; **245**:302–305.

[15] Folkman J. Tumor angiogenesis: therapeutic implications. New England Journal of Medicine. 1971;**285**:1182–1186. doi:10.1056/NEJM197108122850711

[16] Burke PA, DeNardo SJ. Antiangiogenic agents and their promising potential in combined therapy. Critical Reviews in Oncology/Hematology. 2001;**39**:155–171. doi:10.1016/S1040-8428(01)00115-9

[17] Carmeliet P, Jain RK. Angiogenesis in cancer and other diseases. Nature. 2000;**407**:249–257. doi:10.1038/35025220

[18] Rajput MS, Agrawal P. Microspheres in cancer therapy. Indian Journal of Cancer. 2010;**47**:458–468. doi:10.4103/0019-509X.73547

[19] Kennedy AS, Salem R. Comparison of two ^{90}Yttrium microsphere agents for hepatic artery brachytherapy. In: Proceedings of the 14th International Congress on Anti-cancer Treatment; 5–7 February 2013; ICACT, Paris: International Congress on Anti-Cancer Treatment; 2013. pp. 1–156.

[20] Carr BI. Hepatic arterial ^{90}Y glass microspheres (Therasphere) for unresectable hepatocellular carcinoma: interim safety and survival data on 65 patients. Liver Transplantation. 2004;**10**:S107–S110. doi:10.1002/lt.20036

[21] Murthy R, Nunez R, Szklaruk F, Erwin W, Madoff DC, Gupta S, Ahrar K, Wallace MF, Coehn A, Coldwell DM, Kennedy AS, Hicks ME. Yttrium-90 microsphere therapy for hepatic malignancy: devices, indications, technical considerations, and potential complications. RadioGraphics. 2005;**25**:S41–S55. doi:10.1148/rg.25si055515

[22] Kennedy A, Nag S, Salem R, Murthy R, McEwan AJ, Nutting C, Benson A, Espat J, Bilbao JI, Sharma RA, Thomas JP, Caldwell D. Recommendations for radioembolization of hepatic malignancies using Yttrium-90 microsphere brachytherapy: a consensus panel report from the radioembolization brachytherapy oncology consortium. International Journal of Radiation Oncology, Biology, Physics. 2007;**68**(1):13–23. doi:10.1016/j.ijrobp.2006.11.060

[23] Chaudhury PK, Hassanain M, Bouteaud JM, Alcindor T, Nudo CG, Valenti D, Cabrera T, Kavan P, Feteih I, Metrakos P. Complete response of heptocellular carcinoma with sorafenib and ^{90}Y radioembolization. Current Oncology. 2010;**17**(3):67–69.

[24] Dezarn WA, Cessna JT, DeWerd LA, Feng W, Gates VL, Halama J, Kennedy AS, Nag S, Sarfaraz M, Sehgal V, Selwyn R, Stabin MG, Thomadsen BR, Williams LE, Salem R. Recommendations of the American Association of Physicists in Medicine on dosimetry, imaging, and quality assurance procedures for ^{90}Y microsphere brachytherapy in the treatment of hepatic malignancies. Medical Physics**.** 2011;**38**(8):4824–4845. doi:10.1118/1.3608909

[25] Lau WY, Lai EC, Leung TW. Current role of selective internal irradiation with yttrium-90 microspheres in the management of hepatocellular carcinoma: a systematic review. International Journal of Radiation Oncology, Biology, Physics. 2011;**81**(2):460–467. doi:10.1016/j.ijrobp.2010.06.010

[26] Lee IK, Seong J. The optimal selection of radiotherapy treatment for hepatocellular carcinoma. Gut and Liver. 2012;**6**(2):139–148. doi:10.5009/gnl.2012.6.2.139

[27] Amor-Coarasa A, Milera A, Carvajal D, Gulec S, McGoron AJ. ^{90}Y-DOTA-CHS microspheres for live radiomicrosphere therapy: preliminary in vivo lung radiochemical stability studies. Journal of Radiotherapy. 2014;**2014**:1–6. doi:10.1155/2014/941072

[28] Travish G, Yoder RB. Laser-powered dielectric-structures for the production of high-brightness electron and x-ray beams. Proceedings of SPIE**.** 2011;**8079**:80790K–80790L. doi:10.1117/12.890263

[29] Shen WQ,Wang B, Feng J, Zhan WL, Zhu YT, Feng EP. Total reaction cross section for heavy-ion collisions and its relation to the neutron excess degree of freedom. Nuclear Physics A. 1989;**491**:130–146. doi:10.1016/0375-9474(89)90209-1

[30] Barrett KE, Barman SM, Boitano S, Brooks H. Ganong's review of medical physiology. 24th ed. New York: McGraw-Hill Medical; 2012. 752 p.

[31] Bethe H. Zur theorie des durchgangs schneller korpuskularstrahlung durch materie (The theory of the passage of fast corpuscular radiation through matter). Annalen der Physik (Annals of Physics). 1930;**5**:325–400. doi:10.1002/andp.19303970303

[32] Radiation Safety Information Computational Center. Computer code collection: code package CCC-228, SPAR. Calculation of stopping powers and ranges for muons, charged pions, protons, and heavy ions. 1985; Oak Ridge: Oak Ridge National Laboratory.

[33] Rittmann PD. ISO-PC version 2.2-user's guide. 2004; Richland: Fluor Government Group.

[34] IAEA. Relative biological effectiveness in ion beam therapy, International Atomic Energy Agency, IAEA Technical Reports Series, No. 461. 2008; Vienna: IAEA.

[35] Baum EM, Ernesti MC, Knox HD, Miller TR, Watson AM. Nuclides and isotopes chart of the nuclides. 17th ed. 2010; Schnectady: Knowles Atomic Power Laboratory.

[36] National Cancer Action Team. National radiotherapy implementation group report. Image guided radiotherapy (IGRT): Guidance for implementation and use. 2012; London: NCAT.

[37] ICRP Publication 30. Limits for intakes of radionuclides by workers. 1979; Oxford: Pergamon.

[38] Bevelacqua JJ. Basic health physics: problems and solutions. 2nd ed. 2010; Weinheim: Wiley-VCH. 743 p.

[39] ICRP Publication 119. Compendium of dose coefficients based on ICRP publication 60. 2012; Amsterdam: Elsevier.